Influences of Lake Malawi

on the spatial and diurnal variability of local precipitation

Shunya Koseki[1] and **Priscilla A. Mooney**[2]

1: Geophysical Institute, University of Bergen, Bjerknes Centre for Climate Research, Bergen, Norway

2: NORCE Norwegian Research Centre, Bjerknes Centre for Climate Research, Bergen, Norway

Corresponding author: Shunya Koseki

Email: Shunya.Koseki@gfi.uib.no

Address: Allégate 70, 5007, Bergen, Norway

Abstract

We investigate how the intensity and spatial distribution of precipitation varies around Lake Malawi on a diurnal time scale, which can be valuable information for water resource management in tropical southeastern African nations. Using a state-of-the-art satellite product and regional atmospheric model, the well-defined diurnal cycle is detected around Lake Malawi with harmonic and principle component analyses: the precipitation is intense during midnight to morning over Lake Malawi and the precipitation peaks in the daytime over the surrounding area. This diurnal cycle in the precipitation around the lake is associated with the lake-land breeze circulation. Comparisons between the benchmark simulation and an idealized simulation in which Lake Malawi is removed, reveals that the diurnal variations in precipitation are substantially amplified by the presence of Lake Malawi. This is most evident over the lake and surrounding coastal regions. Lake Malawi also enhances the lake-land breeze circulation; the nocturnal lakeward land breeze generates surface convergence effectively and precipitation intensifies over the lake. Conversely, the daytime landward lake breeze generates the intense divergence over the lake and precipitation is strongly depressed over the lake. The lake-land breeze and the background vapour enriched by Lake Malawi drives primarily a diurnal variation in the surface moisture flux divergence/convergence over the lake and surrounding area which contributes to the diurnal cycle of precipitation in this region.

1. Introduction

A key climatological characteristic of tropical southeastern Africa is the manifestation of dry and wet seasons induced by the meridional march of the Inter-tropical Convergence Zone (ITCZ). This seasonal movement in the ITCZ is associated with the southwesterly Indian summer and northeasterly winter monsoons (e.g., Camberlin 1997; Viste and Sorteberg, 2013; Jury 2016; Diallo et al., 2018; Koseki and Bhatt, 2018) as shown in Figs. S1a-l. In summer (May to September), tropical southeasten Africa is covered entirely with a moisture flux divergence (Fig. S1m) and consequently, a dry season falls on this region. The northeastward moisture flux provides some of the summer precipitation over northeastern Africa and South Asia (e.g., Segele et al., 2009a; Viste and Sorteberg, 2013; Gleixner et al., 2017; Bohlinger et al., 2017). Conversely, the southwestward Indian winter monsoon generates a large convergence of vertically-integrated moisture flux over the tropical southeast of Africa (November to March, as shown Fig. S1n) bringing a wet season to this region. This monsoon-brought precipitation is very important for the regional economy and society of the southeastern African nations such as Tanzania, Mozambique, Madagascar, and Malawi where their economies depend highly on rain-fed agriculture.

Variability in hourly rainfall is also dominant over Southeastern Africa. It is controlled largely by a diurnal cycle due to the thermal heat contrast between water surface and land surface in the tropics (e.g., Estoque, 1967; Mak and Walsh, 1976; Kikuchi and Wang, 2008; Teo et al., 2011; Koseki et al., 2013; Jury, 2016). The diurnal cycle is observed ubiquitously around the tropical coastal areas since the thermal contrast between coastal land and ocean during daytime and nighttime, induces the sea and land breeze circulation (e.g., Kitoh and Arakawa, 2005; Kikuchi and Wang, 2008; Teo et al., 2011; Diro et al., 2012; Koseki et al., 2013). Steep terrain and land-lake contrast also generate the similar diurnal variations in precipitation. These variations are associated with the diurnal cycle of mountain-valley and lake-land breeze systems (e.g., Keen and Lyons, 1978; Joseph et al., 2008; Stivari et al, 2003; Crosman and Horel, 2010; Koseki et al., 2018). Such information on diurnal variation in precipitation is highly important for efficient water resource management in nations with economies that depend strongly on rain.

Lake Malawi, located at 12.11°S and 34.22°E (Fig. S1), is the third largest of the African Great Lakes and ninth in the world having an area of 29,600 km^2, a maximum width of 75km, and a maximum length of 560km. Lake Malawi is an important water resource for surrounding tropical southeastern African nations such as Malawi, Mozambique and Tanzania (Kumambala and Ervine, 2010). In particular, a large part of agriculture and energy in Malawi originates from the water resource of Lake Malawi and the Shire River which flows from the lake; all of the national hydropower stations are built on the Shire River (a total installation capacity of 280MW; Kumambala and Ervine, 2010) and the largest national sugar plantations are supplied with water from the Shire River. Societies along the Shire River and surrounding Lake Malawi are exposed to high risks of flooding during the rainy season (November to March, Fig. 1) when the lake level is high due to rainfall over the lake (e.g., Neuland, 1984; Schäfer et al., 2015). Regarding other aspects, Lake Malawi is an important fishing resource in Malawi and it has a very unique ecosystem and biodiversity (e.g., Weyl et al., 2010). Lake Malawi itself plays an important role in the regional climate system. Diallo et al. (2018) performed climate simulations with a state-of-the-art regional climate model and suggested that Lake Malawi is a water source for regional precipitation (over the lake and surrounding area) via intense latent heat flux release from the lake surface.

Although Diallo et al. (2018) have investigated the role of Lake Malawi for monthly time scales, little is known about the diurnal cycle of rainfall around Lake Malawi and the lakes's influence on the diurnal cycle. In general, the African Great Lakes play an important role for the regional hydrological weather and climate system as a large water source. For example, Thiery et al. (2016) showed that Lake Victoria (area of 59,947km^2), which is the largest African Great Lake, triggers extreme thunderstorm over the lake during nighttime. Other exampes include severe snowstorms around the Great Lakes of North America (area of 244,106km^2) (e.g., Sousonis and Mann, 2000; NOrato et al., 2013), and local precipitation induced by Lake Chad (area of 25,000km^2) (Lauwaet et al., 2012). Since Lake Malawi, a large water body (29,600km^2), is located in the tropics, the region can be affected by the strong diurnal cycle of incoming solar radiation (e.g., Crosman and Horel, 2010). This is the main driver of the diurnal variations in precipitation and local breeze systems. Although it is expected that Lake Malawi can drive local circulation in response to the diurnal solar radiation, the lake's role in the diurnal cycle of precipitation is less clear and poorly understood. This is partly due to the lack of tools to study this topic but recent developments in the resolution of numerical models now permit such investigations.

This study aims to investigate the regional diurnal cycle of precipitation in the rainy season (November to March) and quantify the effects of Lake Malawi on the diurnal cycle of precipitation using state-of-the-art observational products and numerical regional model. Using a satellite product with a relatively coarse spatial resolution, a climatological diurnal cycle is overviewed and a case study of November to March in 2014/15 is investigated using a higher resolution satellite product for the purpose of evaluating the numerical simulation.

The rest of this paper is structured as follow: Section 2 gives the details of observational data and numerical model used in this study and statistical methodologies to investigate the diurnal variations. Section 3 provides the results of the statistical analysis on the observations and numerical simulation including an assessment of the modeled diurnal cycle. Moreover, the results of an idealized numerical experiment will be used to elucidate the physical mechanisms that underlie Lake Malawi's role in the diurnal cycle of precipitation around the lake. Section 4 will discuss the details of the simulation results focusing on the quantification of the influence of Lake Malawi and finally, we will summarize this study in Section 5.

2. Data, Model, and Methodology

2.1 Observational Data

Satellite observations are obtained from both the Tropical Rainfall Measuring Mission (Huffman et al., 2007) version 3B42 (TRMM 3B42) and the Global Precipitation Measurement (GPM, Skofronick-Jackson et al., 2017) mission data (Level-3). TRMM 3B42 has a high temporal coverage (1998-2014) which facilitates a climatological overview of the diurnal cycle over Lake Malawi. However, the spatial resolution of TRMM 3B42 (0.25°) prohibits its use in the analysis of the spatial characteristics of the diurnal cycle over the lake and its shores. This difficulty is overcome by using GPM, the successor to TRMM 3B42, which has a higher spatial resolution of 0.1°. This facilitates a more detailed study of spatial variations in the diurnal cycle of precipitation. The temporal resolution of the original GPM Level-3 data is every 30 minutes which is averaged to hourly rainfall in this study.

2.2 Weather Research and Forecasting (WRF) Model

The Advanced Research Weather Research and Forecasting (hereafter referred to WRF, Skamarock et al., 2007) model version 3.9.1 is used to investigate the diurnal variations around Lake Malawi. The domains used in all simulations are shown in Figure 1a. The outer domain covers southeastern Africa, -20.74902°S to -2.958107°S and 23.3115°E to 44.0885°E with 15km grid spacings (171×117 grids) and the inner domain is centred on Lake Malawi, -15.87943°S to -8.219772°S and 32.22042°E to 37.06839°E with 3km grid spacing (155×250 grids), respectively (Fig. 2a). Both domains have 56 vertical layers. The outer domain is forced laterally with 6 hourly ERA-Interim (Dee et al., 2011) data which has a grid spacing of 0.75° and at the lower boundary by the daily Optimum Interpolated Sea Surface Temperature (OISST, Reynolds et al., 2007) which has a grid spacing of 0.25°. The inner domain is forced laterally by the outer domain of WRF (the outer domain of WRF does not interact with the inner domain).

The following physical schemes are used in our WRF simulations: the WRF Single-moment (WSM) 6-class scheme for microphysics (Hong and Lim, 2006) and the Yonsei University parameterization for the Planetary Boundary Layer (PBL; Hong et al., 2006). The longwave and shortwave radiative forcing are parameterized by the Rapid Radiative Transfer Model (Mlawer et al., 1997) schemes. Betts-Miller-Janjíc (Janjíc, 1994) scheme is used for parameterizing convective processes in the outer domain only; cumulus parameterization is switched off in the convection permitting inner domain. A study of the sensitivity of precipitation in this region to the convective schemes used in the outer domain showed that simulations using the Betts-Miller-Janjíc scheme reproduced the observed precipitation over land better than simulations using the Kain-Fritsch (Kain, 2004) scheme (not shown). Therefore, the Betts-Miller-Janjíc scheme is chosen for the outer domain in this study with no cumulus scheme used in the inner, high-resolution domain. Over the land and lake grids that are based on MODIS landuse data, the NOAH land surface model consisting of 4-layers (Chen and Dudhia, 2001a, b) and the 9-layer lake model (Xu et al., 2016) are implemented and air-land/lake interactions are active in the simulations.

With the model configurations above, a control experiment is initialized on the 1st January 2014 at 00 UTC of ERA-Interim for atmosphere and land surface and integrated until April 1st of 2015 (referred to WRF-CTL, hereafter). This run will compliment the observations to gain insights into the diurnal variations around Lake Malawi. In a second experiment, the grid boxes over Lake Malawi are converted from water to land grid boxes (Figs. 1b and c). This facilitates an exploration of the role of Lake Malawi on the local diurnal variations (called WRF-NOLM in the rest of the paper). Due to this conversion, some land surface properties are modified in WRF-NOLM: the landuse index of the converted grids is set to be savanna which is the most dominant landuse category in the inner domain of WRF experiments. The soil type of the converted grids is also replaced with sandy clay loam which is the majority soil type for the savanna grids in the inner domain. Additionally, the surface albedo over Lake Malawi grids is set to a value of albedo averaged over the savanna grids in the inner domain. Finally, the soil moisture and temperature of the converted grids are initialized by averaged value of savanna grids. These modifications are done only in the inner domain to avoid any modulations in larger-scale meteorological and hydrological quantities associated with the absence of Lake Malawi. All settings of the outer domain of WRF-NOLM are exactly the same as those of WRF-CTL.

We analyze the hourly output of the 5 months from November in 2014 to March in 2015; that is the first 10 months are designated as a spin-up period for initialising the land surface following the methodologies of Cosgrove et al. (2002) and Chen et al. (2007). In particular, in WRF-NOLM, the soil moisture and temperature are initialized with an averaged value, which is to a large extent artificial. Therefore, a long spin-up period is employed for initialising the land surface.

2.3 Methodologies to detect the nature of diurnal variation

Harmonic analysis has been widely used to quantify the main characteristics of the diurnal cycle (e.g., Yang and Slingo, 2001; Diro et al., 2012; Mooney et al., 2017). One particular advantage of harmonic analysis is the estimation of the explained variance (%) of a specific frequency and its phase from a time series. This study follows Mooney et al. (2017) by fitting the following function to the NDJFM-averaged hourly data,

$$R(t) \cong a_{24}\cos\left(\frac{2\pi(t-\phi_{24})}{24}\right)+a_{12}\cos\left(\frac{2\pi(t-\phi_{12})}{12}\right) \qquad (1),$$

where $R(t)$ is the hourly variation of total rainfall and a_{24} (a_{12}) and ϕ_{24} (ϕ_{12}) are the amplitude and phase of the diurnal and semi-diurnal cycle, respectively.

The empirical orthogonal function (EOF) analysis is additionally used to capture the features of the diurnal cycle around Lake Malawi following previous studies (e.g., Kikuchi and Wang, 2008; Teo et al., 2011).

The EOF analysis is used to identify the dominant spatio-temporal patterns. For the diurnal cycle, it is known that the first mode represents a stationary dipole pattern between coastal land and ocean while the second mode identifies a propagation pattern from land to sea (the EOF patterns and principle component scores between the first and second modes are out of phase by approximately $\pi/4$, e.g., Kikuchi and Wang, 2008; Teo et al., 2011). Employing these statistical methodologies, we will explore the details of the observed and modeled diurnal cycle around Lake Malawi in Section 3.2 and 3.3. The EOF analysis is adopted into the diurnal deviation components with,

$$A'(t) = A(t) - \overline{A} \qquad (2),$$

where A is a variable and t is time (hourly). The overbar and prime denote the daily-mean and daily-deviated components, respectively.

3. Results

In this section, we will show the essential features of diurnal cycle of precipitation around Lake Malawi using satellite observations and WRF simulations. Additionally, the results of the idealized WRF simulation will be compared and contrasted with the control simulation to reveal the role of Lake Malawi in the local diurnal cycle of precipitation.

3.1 Climatology

Firstly, we take an overview of the climatological diurnal cycle of precipitation around Lake Malawi using TRMM 3B42 which has good temporal coverage but relatively coarse resolution (temporarily and spatially). Figure 2 illustrates the 3-hourly precipitation obtained by TRMM-3B42 for NDJFM-mean climatology. Between 00-03 to 06-09 UTC (02-05 to 08-11 LST), the precipitation over Lake Malawi is enhanced and the precipitation over the surrounding land area becomes weaker. At 09-12 UTC, the precipitation is suppressed over the entire area. Later, from 12-15 LST, precipitation is activated over the land surrounding Lake

Malawi. The land precipitation intensifies widely at 15-18 UTC while rainfall over Lake Malawi is negligible. From 18-21 to 21-00 UTC, the land precipitation is gradually reduced and precipitation over Lake Malawi commences. That is, around Lake Malawi there is a well-organized diurnal variation in precipitation. Interestingly, the magnitude of land and lake precipitation is almost identical (0.9 mm/h).

3.2 Case study, 2014/15 NDJFM

In this subsection, the more detailed nature of the diurnal cycle, which is indicated in the preceding subsection, is investigated with a finer resolution satellite product and numerical simulation for a case study of November to March in 2014/15. Figures 3a-e show monthly-mean rainfall for GPM from November to March. In November, the daily rainfall around Lake Malawi is low compared to the other months. There is little rainfall over the Southern part of Lake Malawi but there is some intense rainfall over the northern part of the lake. Rainfall becomes more intense in December particularly over the centre of Lake Malawi. Precipitation peaks in January and it is very intense in the entire domain with rainfall over Lake Malawi reaching ~ 22 mm/h. From February to March, the precipitation over land decreases while the lake precipitation over the lake remains strong, especially, in the central area (around 18 mm/h). The precipitation over Lake Malawi is not distributed homogeneously, but it seems that there is a dependency on location: the precipitation is intense in the central part of the lake in December to March, in particular, the precipitation spreads broadly around the centre of the lake. In the northern and southern edges of the lake, there are also moderate peaks of the precipitation in Feruary and March. These distributions might be determined by several factors (for example, lake surface temperature), which is a highly complex process and beyond the scope of this study. Fig. 3f-j show that WRF-CTL can capture the seasonal march of larger-scale precipitation. However, the land precipitation tends to be overestimated, in particular, from January to February. This overestimation might be due to the high topography (higher than 2300m) around Lake Malawi (see section 4). WRF-CTL successfully reproducse the intense lake precipitation from November to March.

3.3 Harmonic analysis

Figure 4 shows the key characteristics of the diurnal cycle of precipitation obtained by harmonics analysis (see Section 2.3) for NDJFM-mean hourly data of GPM and WRF-CTL. Over Lake Malawi, the GPM observed sub-daily variations are dominated by the diurnal cycle as shown in Fig. 4a (about 70-80% of explained variance). Other dominant diurnal cycles are seen along the coast of Lake Malawi and to the northeast of Lake Malawi, around 10°S and 35-36°E with a similar explained variance. In WRF-CTL the dominant diurnal variation are captured well over Lake Malawi with 60-70 % of explained variance in Fig. 4e. Although the strength of the diurnal signal over the coastal region tends to be underestimated to some extent, the terrestrial diurnal cycle is well represented in WRF-CTL in terms of the explained variance.

The largest amplitudes of the diurnal cycle (a_{24} in Eq. 1) are observed over Lake Malawi (up to 0.5 mm/h) and its coastal region (Fig. 4b). Over land, the amplitude is relatively large to the northeast of the Lake (0.2-0.3 mm) where the diurnal cycle dominates the sub-daily variations (Fig. 4a). This distribution of amplitude is fairly well simulated by WRF-CTL in Fig. 4f. However, over Lake Malawi, the amplitude is lower than observed while the amplitude over land to the

Northeast is too large (0.5 mm). This is consistent with the overestimated monthly-mean precipitation in Fig. 3. The observed phase of the diurnal cycle (ϕ_{24} in Eq. 1) shows a clear contrast over the lake and land in Fig. 4c; the maximum peak of the precipitation is at 02-03 UTC over the lake and surrounding coastal area and at 13-14 UTC over the land north of the lake where terrestrial precipitation is relatively large (Figs. 4a and b). This result is consistent with the climatological overview in the previous subsection. The timing of the WRF-simulated diurnal cycle in Fig. 4g agrees reasonably with that of the observations. Over the lake, the peak time is slightly late especially in the south (at 03-05 UTC) compared to the observations and the land precipitation is maximized at 13-14 UTC to the north of the lake. However, over the central eastern coastal region, the timing of the rainfall is incorrectly simulated.

In Figs. 4d and h, the explained variance of semi-diurnal cycle is given for GPM and WRF-CTL. Neither product shows a clear semi-diurnal cycle around Lake Malawi although there are some spots with relatively high variance of 40-50 %. These results suggest that the sub-daily variations in rainfall are mainly associated with the diurnal cycle over and around the lake while semi-diurnal cycle is almost negligible.

Figures 4i-l show the characteristics of the diurnal cycle of precipitation calculated by the harmonic analysis (Eq.1) for WRF-NOLM. Compared to WRF-CTL (Fig. 4e), the explained variance of the diurnal cycle is almost identical around Lake Malawi, in particular, to the northeast of the lake. Over the lake, the variance of the diurnal cycle is reduced remarkably in the southern part of the lake, which drops down to 20-30% in Fig. 5i (50-60% in WRF-CTL, shown in Fig. 4e). To the north of the lake, the diurnal cycle persists despite the absence of the lake. However, the amplitude of the diurnal cycle shrinks over the entire lake in Fig. 4j. Most notably, the reduction is largest in the central part and the northern part of the lake (a decrease from 0.5 mm/h to 0.1-0.2 mm/h) even though the variance of the diurnal cycle is still comparable to the WRF-CTL case. Over land, the diurnal amplitude is largely unchanged when Lake Malawi is removed; this is most evident overland to the northeast of the lake. The phase of the diurnal cycle is also modified over the lake. Its peak is slightly earlier (around 02-03 UTC) than WRF-CTL (comparison between Fig. 4g and 4k). In the southern shore of the lake (where the diurnal cycle almost disappears), the phase is noisy with respect to WRF-CTL. The component of the semi-diurnal cycle is almost identical with that in WRF-CTL and the semi-diurnal cycle is not of importance in the sub-daily variations (Fig. 4l).

3.4 EOF analysis

The dominant spatio-temporal pattern of variation is provided through the EOF analysis in Fig. 5. The EOF first mode of GPM shows a clear contrast between the land and lake (Fig. 5a). The amplitude is larger over the lake than over the land suggesting that the lake rainfall is more intense than the land rainfall. The coastal land rainfall synchronizes with the lake rainfall in both eastern and western shores. This mode explains 53.69 % of the total variance and its principal component (PC) score (Fig. 5h) shows a distinct diurnal cycle. The peak of rainfall over land is between 12-17 UTC and that of the lake rainfall over the lake is between 23-03 UTC. This seesaw pattern of daytime rainfall over land and nighttime rainfall over the lake is quite similar to the pattern described by sea-land contrast in the tropics (e.g., Teo et al., 2011; Bhatt et al., 2016). The EOF second mode has 15.77% of the total variance and its spatial pattern and PC score do not indicate a propagation mode from land to lake (not shown). The PC score seems a semi-diurnal cycle and the spatial pattern is quite spotty and it appears to be unrelated to Lake Malawi. Its amplitude is considerably smaller than that of the first mode.

WRF-CTL represents well the sharp contrasting spatial pattern between the land and lake in Fig. 5b as an EOF first mode (the explained variance is 41.51%). However, as shown in Figs. 3 and 4, the amplitude of the land precipitation is overestimated and coastal terrestrial rainfall synchronizing with the lake rainfall does not spread widely compared to the observation although there is some coastal land precipitation occurring simultaneously with the lake precipitation. While the PC score of first mode is roughly consistent with that of observation (Figs. 5h and i), the phase is somewhat shifted: the peak of the nighttime rainfall is around 03-07 UTC (later than the observation) and that of daytime is around 12-14 UTC, which is slightly earlier than the observation. In particular, the earlier simulated peak in the daytime precipitation is a common issue in regional climate modeling (e.g., Nikulin et al. 2012; Pohl et al., 2014; Mooney et al., 2016, 2017; Koseki et al., 2018). Similar to the GPM observations, WRF-CTL does not show any clear propagation mode by the second mode and the large variation is limited in some small areas (its variance is 18.36 %) although the PC score of the second mode is lagged by approximately $\pi/4$ (not shown).

The modeled surface zonal wind shows an interesting distribution by the EOF first mode in Fig. 5c: the lake shore is encompassed by the narrow bands of the negative and positive daily anomalies of surface zonal wind (77.88% of the total variance) and those bands spread over Lake Malawi. Combined with its PC score it can be interpreted that the outgoing flow from the Lake is maximized between 09-13 UTC (Fig. 5i) and the incoming flow into the Lake is dominant between 21-03 UTC. This diurnal-varying circulation is consistent with a well-characterized lake-land breeze (e.g., Keen and Lyons, 1978; Crosman and Horel, 2010). The PC score of the surface zonal wind leads that of the precipitation by approximately 3 hours. The surface meridional wind also shows a remarkable pattern by the EOF first mode (61. 46% of the total variance) in Fig. 5d: with a macroscopic view, there is a dipole mode of positive in the north and negative in the south of Lake Malawi. Combining it with the PC score (Fig. 5i), there is an outgoing/incoming flow of meridional surface wind during daytime/nighttime respectively. The EOF 1st mode of meridional wind varies approximately with the zonal wind as shown in Fig. 5i.

The EOF 1st mode also shows substantial changes in the diurnal cycle in WRF-NOLM as shown in Figs. 5e-g; the dipole pattern between the lake and surrounding terrestrial area almost disappears in the EOF 1st mode and the dominant variability is only over the land in Fig. 5e. The variance is still 35.60% and the amplitude over the land is almost identical with that of WRF-CTL in Fig. 5b. While the harmonic analysis estimates the diurnal cycle independently at each grid cell, the EOF analysis calculates the most explainable variability in all the selected grids and therefore, the amplitude at one grid would be affected by that at other grids. That is, in Fig. 5e, the variability at the lake grids are much smaller than those at land grids, which is consistent with the reduced amplitude of diurnal variation over the lake in Fig. 4j. The PC score indicates that the EOF 1st mode is a diurnal cycle in Fig. 5j with some modification in its peak time. Whereas the EOF 1st mode of surface zonal winds have the two narrow bands along the lake shore in WRF-NOLM (74.53% of the total variance), their spreads over the lake are largely diminished on both sides of the lake shore with respect to that in WRF-CTL (Figs. 5c and 5f). The magnitudes of the WRF-CTL (Fig. 5i) PC scores are similar to those for WRF-NOLM (Fig. 5j) and the maximum and minimum of the PC scores for both WRF-CTL and WRF-NOLM occur during the day and the night, respectively. Similarly, the variability in surface meridional wind is also reduced over the lake as shown in Fig. 5g. However, there is still some evidence of a dipole pattern between the northern and southern part of Lake Malawi as shown in WRF-CTL (Fig. 5d). However, the maximum of PC scores for the meridional wind occurs slightly earlier in the WRF-NOLM (Fig. 5j) simulation compared to the WRF-CTL (Figs. 5i).

3.5 Nighttime and daytime precipitation

As witnessed by the harmonic and EOF analyses above (Figs. 4-5), Lake Malawi plays a crucial role in the generation and/or amplification of the diurnal cycle of precipitation. At certain times in the day, the lake's role can be clearer than other times (Fig. 6). During 00-03 UTC, the nocturnal precipitation occurs over Lake Malawi in WRF-CTL (Fig. 6a) but this the lake-anchored precipitation is extensively reduced in WRF-NOLM (Fig. 6b). Its influence is remarkable over the entire lake, in particular, over the northern and central parts of the lake (Fig. 6c). This indicates the importance of Lake Malawi for rainfall over the lake (as concluded by Diallo et al., 2018). Conversely, the surrounding area of the lake experiences a modest reduction in precipitation in the presence of the lake during midnight to early morning. During daytime when the precipitation peak is closely tied to the maximum in local solar heating (11-14 UTC), precipitation is more dominant over the surrounding area of the lake than over the lake in WRF-CTL (Fig. 6d). While precipitation over the lake is quite small, there is some increase in the precipitation over the southern part of the lake in WRF-NOLM, (Fig. 6e). In contrast to the nocturnal precipitation, daytime precipitation is amplified over the southern part of the lake although its response is relatively weaker than that in the nighttime (Figs. 6c and f).

Figure 7 presents the surface horizontal wind and its divergence anomalies from daily-mean at nighttime and daytime, estimated by Eq. (2). In WRF-CTL, the incoming flow from the shore toward the lake is detected and the strong convergence forms over the lake shown in Fig. 7a. These lakeward flows are land breeze circulations and penetrate deeply into the lake as shown by the EOF analysis (Figs. 5c and d). The intense nocturnal rainfall (as in Fig. 6a) can be attributed to this strong convergence over the lake. In WRF-NOLM, the land breezes are extensively weakened and, as a result, the convergence over the lake shrinks considerably (Fig. 7b). The difference shows clearly that the intensification in the land breeze and convergence is due to Lake Malawi (Fig. 7c). While the daily-residual component of the surface wind can be seen not only around the lake but also in the region (Figs. 7a and b), the influence of the lake on the wind seems to be limited around and over the lake. During daytime, on the other hand, the outgoing flows, thus, lake breezes are organized well from the lake outward and this flow is highly divergent over the lake in WRF-CTL (Fig. 7d). This outgoing circulation can also be seen in WRF-NOLM (Fig. 7e), but its magnitude is considerably reduced and the flow-forming divergence is also reduced. The difference during daytime is almost a mirror image of that during nighttime and it shows that Lake Malawi plays an important role in the diurnal variations of local wind circulations. The lake surface seems to create a heat contrast favouring the lake-land breeze circulation in night- and daytime: the surface temperature over the lake is higher in WRF-CTL (25.7^{o}C) than in WRF-NOLM (24.8^{o}C) during nighttime and lower in WRF-CTL (26.8^{o}C) during the daytime than in WRF-NOLM (32.8^{o}C) This behaviour in the surface temperature can create favourable conditions for more convergence (divergence) and consequently, the precipitation over the lake is enhanced (suppressed) effectively.

3.6 Moisture flux convergence

The preceding subsections have shown that Lake Malawi radically drives the diurnal cycle in precipitation, and local circulations. Since the moisture flux, $\mathbf{U}q$, (here, $\mathbf{U}$ is horizontal wind vector and q is specific humidity at surface) due to the lake-land breeze circulations can be highly related to precipitation, we quantify the surface moisture flux and its diurnal variation. Note that 10m and 2m data are used for horizontal wind and specific humidity in this study. The moisture flux can be subdivided into four components like,

$$\mathbf{U}q(t) = \left(\overline{\mathbf{U}} + \mathbf{U}'(t)\right) \cdot \left(\overline{q} + q'(t)\right) = \overline{\mathbf{U}}\overline{q} + \overline{\mathbf{U}}q'(t) + \mathbf{U}'(t)\overline{q} + \mathbf{U}'(t)q'(t),$$

where the overbar and prime denote daily-mean and daily-deviation as Eq. 2. $\mathbf{U}$ is surface wind vector and q is surface specific humidity. The horizontal divergence of moisture flux is calculated as

$$\nabla \cdot \mathbf{U}q(t) = \underbrace{\nabla \cdot \overline{\mathbf{U}}\overline{q}}_{A} + \underbrace{\nabla \cdot \overline{\mathbf{U}}q'(t)}_{B} + \underbrace{\nabla \cdot \mathbf{U}'(t)\overline{q}}_{C} + \underbrace{\nabla \cdot \mathbf{U}'(t)q'(t)}_{D} \quad (3).$$

The term A is the moisture flux divergence/convergence due to daily-mean wind and humidity, which does not have diurnal variation, but its relevance is more to the moisture flux associated with the Indian winter monsoon over this region. The term B reflects the influence associated with the diurnal variation in the heat flux and the background wind. The term C indicates the contribution due to the lake-land breeze and the daily-mean humidity to the moisture flux divergence/convergence. The final term is attributed to the diurnal variations in local breeze and humidity. Since the term A does not contain any temporal change, only the three terms of B, C, and D are averaged over Lake Malawi and surrounding area as shown in Fig. 8a.

During nighttime, the moisture flux converges over Lake Malawi and diverges over the surrounding area mainly by the lake-land breeze circulation and background humidity in WRF-CTL (term C in Figs. 8b and c). The daily-mean (background) latent heat flux averaged over the lake grids is 155.2572 and 56.9174 W/m^2 for WRF-CTL and WRF-NOLM, respectively and the lake surface is an important water source of the local precipitation, depending on the wind conditions and other characteristics (e.g., topography). The intense moisture flux convergence is responsible for the nocturnal precipitation as shown in Fig. 8c. Other terms in Eq.3 do not substantially contribute to the moisture flux divergence/convergence. In WRF-NOLM, the diurnal varying breeze and background humidity also contributes to the moisture flux convergence/divergence, but its magnitude is much smaller than that in WRF-CTL in Figs. 8b and c. Consequently, the precipitation over the lake area is reduced without Lake Malawi. As shown in Fig. 6c, the precipitation surrounding the lake is somewhat enhanced in WRF-NOLM during nighttime (although the response of the rainfall is noisy and weak, the consistency with the response of the moisture flux is reasonable). During daytime, the lake-land breeze and background humidity are still the main driver of the moisture flux divergence/convergence over the lake and surrounding area in Figs. 8d and e. Without the lake, the divergence over the lake and convergence over the lake shore are weakened, which is consistent with the enhanced (reduced) daytime rainfall surrounding (over) the lake in WRF_CTL in Fig. 6f. The term C is mainly contributed by the zonal component, $\partial(uq)/\partial x$, which is about 70 to 80 % of the total divergence/convergence (not shown).

In both cases of nighttime and daytime, the other terms of B and D in Eq.3 do not contribute to the diurnal changes in moisture flux divergence/convergence. That is, the land-lake breeze and the enriched background water vapor due to Lake Malawi mainly drive the diurnal variations in surface moisture flux and consequently, the precipitation around Lake Malawi.

4. Discussion

The previous section has revealed that Lake Malawi plays a vital role to form the diurnal variations in land-lake breeze systems and correspondingly, the precipitation. However, the diurnal cycle of surface winds do not completely disappear in WRF-NOLM, and there is still a signature of the diurnal cycle detected even in the absence of the lake. We provide a brief discussion on the possible other factors of the diurnal cycle around Lake Malawi.

While Lake Malawi is an active driver of the diurnal variations in the local land-lake breeze circulations, the local breeze circulation residually remains without Lake Malawi as shown in Fig. 7. As previous research (e.g., Tyson 1968a, 1968b and Koseki et al. 2018) has shown, complex terrain also induces a diurnal cycle in the mountain-valley breeze circulation whose mechanism is similar to that for sea-land and lake-land breezes. As shown in Fig. 9a, Lake Malawi is encompassed by the high-elevated terrain that is up to 2600m in the northeast. The altitude is below 600 m over all of Lake Malawi. This difference in the elevation forms the large gradients in the surface as shown in Figs. 9b and c. In particular, the two narrow bands of steep zonal gradient run along the eastern and western shore sides. These gradients can drive the down-hill mountain (incoming toward the lake) and uphill valley (outgoing from the lake shore) breeze circulations during nighttime and daytime respectively as shown in Fig. 5b, 7c and 7f. In addition to the lake shore, there are some steep gradients to the northeast (9°S and 34.5°E) and the southwest (14.5°S and 33.5-34.5°E). Around these high mountains, there are well-organized mountain and valley breeze circulation during nighttime and daytime as in Figs. 7a, b, d and e. The daytime precipitation is enhanced around these regions, that is, the valley breeze can activate the cumulus convection and precipitation due to the topography-lifting effect (e.g., Joseph et al., 2008). The overestimated precipitation in the WRF simulations might be caused by an over sensitive response in convection to this valley breeze circulation.

As previously mentioned, the high topography around Lake Malawi can be another driver of the diurnal cycle around Lake Malawi. However, there could be some difference in timing between the diurnal cycle induced by the lake and mountain due to the difference in heat capacity. Therefore, in WRF_NOLM where the mountain is only a driver, the peak time of precipitation over the lake differs from that in WRF_CTL. That is, the diurnal cycle around Lake Malawi is a complicated system influenced by both the lake and the mountain. Similar mechanisms can be expected in other places where large lakes are surrounded by high mountains (e.g., Lake Tanganyika in Tanzania). Future work will investigate explicitly the role of high terrain in diurnal cycle of precipitation.

In our sensitivity experiment, we used only one land cover type and one soil type in the lake grid cells. This can slightly infleuce our results, as previous research (e.g., Bonan, 2008) has shown that changing the land cover from forests to open spaces (e.g., savanna or croplands) impacts precipitation and temperature. These differences are driven by changes in parameters associated with each land cover type, such as, albedo, surface roughness, leaf area index, and root depth. In tropical regions, changes from forest cover to grass decreases precipitation and increases temperature by changing the partitioning of the net surface radiation between latent and sensible heat fluxes (Bonan, 2008; Pitman et al., 2011). In particular, Semazzi and Song (2001) showed that changing the land cover type from forest to savanna grasslands reduced precipitation over Mozambique. Consequently, changing the lake cover to a tropical forest instead of svanna in our WRF-NOLM simulation would increase the daytime precipitation in WRF-NOLM, potentially, altering the amplitude of the diurnal cycle. However, it is unlikely that changing the land cover type to forest would impact the phase of the diurnal cycle. Based on this, we hypothesise that changing the lake to a forest cover type instead of savanna in WRF-NOLM, would likely result in slightly smaller differences between WRF-CTL and WRF-NOLM with respect to the amplitude of the diurnal cycle of precipitation but it would have no impact on the phase of the diurnal cycle of precipitation. However, further studies on the importance of the land cover change to the diurnal cycle of precipitation would be necessary to test this hypothesis.

Cumulus convection and associated precipitation are also highly sensitive to and modulated by soil moisture whose features are dependent on land use and soil type (e.g., Walker and Rowntree, 1977; Pielke, 2001; Cook et al., 2006). For example, Sugimoto and Takahashi (2017) suggested that the wetter soil moisture tends to inhibit cumulus convection due to a lower sensible heat flux in South Asia during Indian Summer Monsoon period. In our focusing area, the Indian Winter Monsoon prevails and therefore, it can be anticipated that our results of precipitation and cumulus convection will be changed when the different landuse and soil type are employed in the lake grid cells. Additionally, we have tested only the homogenous distribution of landuse and soil type in the lake grid boxes for the sensitivity experiment. The heterogeneous distribution will modify the distribution of precipitation over the lake. Therefore, further sensitivity experiments with difference land use and soil type would be also interesting to investigate the characteristics of the precipitation and land-atmosphere interactions in this region.

5. Concluding Remarks

In this study, we have investigated the diurnal variation of precipitation in summer (November to March) around Lake Malawi using the state-of-the-art satellite products and regional climate model. In a climatological view, TRMM-3B42 shows a clear diurnal cycle of precipitation around Lake Malawi: the precipitation over the lake is more enhanced during midnight to early morning while the surrounding land area experiences a daytime peak with identical amplitudes between the two phases. Such clear contrast between daytime rainfall over the land and nighttime rainfall over the lake can be found over Lake Victoria (Thiery et al., 2016), which is the largest great lake in the African Continent.

The spatially and temporally finer resolution satellite data of GPM and a convection permitting WRF simulation gives a more microscopic view of the diurnal varying precipitation in the area. A harmonic analysis reveals that the diurnal cycle of precipitation is largely dominant over Lake Malawi and to the northeast of the lake and their peak times are almost completely out of phase as suggested by TRMM-3B42. The WRF simulation can capture the diurnal variation in precipitation and reproduce realistic amplitudes of the lake rainfall whilst the land rainfall is overestimated. Analysis of the semi-diurnal cycle shows that the semi-diurnal component is a negligibly small contributor to the diurnal variations. The dominant diurnal variation can also be detected by the EOF analysis as a first principal component (the variance is almost half of the total variance). However, the second modes are not propagating pattern like those identified in Kikuchi and Wang (2008) and Teo et al. (2011). The surface winds also have the dominant first mode of EOF as diurnal cycle. In particular, the lake-land breeze system is well generated along the lake shore.

Without Lake Malawi, those diurnal variations in precipitation and lake-land breeze are diminished substantially around Lake Malawi: a large part of the diurnal variation in precipitation disappears over the lake region. The magnitude of the lake-land breeze reduces its magnitude over the lake. During nighttime, the land breeze does not penetrate deeply into the lake surface and convergence is not formed effectively. During daytime, the outgoing lake breeze also shrinks and the divergence over the lake is weakened considerably. As a result, the daytime rainfall over the surrounding area becomes relatively moderate in the absence of the lake. Basically, Lake Malawi creates a thermal contrast between the lake and land surface and this contrast can drive a local lake-land breeze circulation (e.g., Steyn 2003; Kruit et al., 2004; Crosman and Horel, 2010). As Diallo et al. (2018) suggested, Lake Malawi is a source of water vapour and enhances the precipitation. The combination of lake-land breeze and enriched background water vapour is the main contributor to the diurnal cycle the surface moisture flux and consequently that in the precipitation.

Besides Lake Malawi, the steep gradient associated with high topographies encompassing Lake Malawi also induces a diurnal cycle in the local circulation of the mountain-valley breezes. Due to this breeze system, the diurnal cycle of the terrestrial rainfall survives with identical amplitude in the presence and absence of Lake Malawi. That is, the diurnal variation around Lake Malawi forms a combination of the two independent systems of lake-land and mountain-valley breezes.

Based on the analysis of satellite observations and numerical simulations, we conclude that Lake Malawi plays a central role in the remarkable diurnal cycle of precipitation and local circulation in summer. Such information is useful for other fields such as agriculture and hydropower energy to have more efficient water resources management. For example, Kumambala and Ervine (2010) reviewed the water resources related to Lake Malawi and Shire River and its sensitivity of future climate change using water balance models (e.g., Kebede et al., 2006). The diurnal variations in precipitation can influence the variables of water balance model such as rainfall, lake level and outflow from the lake directly. Therefore, our new findings in this study are informative to the community of water balance models for more accurate estimation of water resources of Lake Malawi.

This study is mainly a case study in only one particular year. Therefore, longer studies on the interaction of large-scale monsoon circulations with the diurnal cycle would be highly desirable. Further analysis should be undertaken on the climate variability of the large-scale monsoon circulation and its impacts on the diurnal cycle of precipitation, and the associated terrestrial hydrological processes. Thiery et al. (2016) have shown that the extreme rainfall due to Lake Victoria is modified by future climate change. Since Lake Victoria and Lake Malawi are located in the same tropical region, similar influence of lake-induced precipitation can be expected. Such insights can help mitigate natural disasters of flooding and drought in this region.

Data availability

The data of TRMM, GPM and ERA-Interim used in this study is able to be downloaded from https://pmm.nasa.gov/data-access/downloads/trmm, https://pmm.nasa.gov/data-access/downloads/gpm, and https://www.ecmwf.int/, respectively. The data of WRF simulations are available from the authors on request.

Author Contribution

SK and PAM made a plan of this work (usage of observational and the experimental designs of WRF simulation) and SK conducted the WRF simulations. SK and PAM contributed to analyze the data. SK wrote a first draft and PAM improved it. The final version of this paper was contributed equally by SK and PAM.

Acknowledgement

The authors greatly appreciate two reviewers, Dr. Ryan Teuling and Dr. Femke Jansen at Wageningen University for their quite constructive and useful comments on the manuscript. The computational resource of this study is supported by Norwegian High-Performance Computing Program resources (NN9039K, NS9039K, NN9385K, NS9207k). S. Koseki is supported by the European Union Seventh Framework Programme (EU-FP7/2007-2013) PREFACE (Grant Agreement No. 603521), ERC STERCP project (Grant Agreement No. 648982), and from the Research Council of Norway (233680/E10). P. A. Mooney gratefully acknowledges funding from the Research Council of Norway (Grant No. 268243).

Reference

Bhatt, B. C., Sobolowski, S., and Higuchi, A.: Simulation of Diurnal Rainfall Variability over the Maritime Continent with a High-Resolution Regional Climate Model. *J. Meteorol. Soc. Jpn*., **94A**, 89-103, doi:10.2151/jmsj.2015-052, 2016.

Bohlinger, P., Sorteberg, A., and Sodemann, H.: Synoptic conditions and moisture sources actuating extreme precipitation in Nepal. *J. Geophys. Res. Atmos*., **122**, 12,653-12,671, doi:10.1102/2017JD027543, 2017.

Bonan, G. B.: Forests and Climate Change: forcings, feedbacks and climate benefits of forests. *Science*, **320**, 1444-1449, 2008.

Camberlin, P.: Rainfall Anomalies in the Source Region of the Nile and Their Connection with the Indian Summer Monsoon. *J. Climate*, **10**, 1380-1392, 1997.

Chen, F., and Dudhia, J.: Coupling an advanced land-surface/hydrology model with the Pen State/NCAR MM5 modeling system. PartI: model description and implementation. *Mon. Wea. Rev.*, **129**, 569-585, 2001a.

Chen, F., and Dudhia, J.: Coupling an advanced land-surface/hydrology model with the Pen State/NCAR MM5 modeling system. PartII: model validation. *Mon. Wea. Rev.*, **129**, 587-604, 2001b.

Chen, F., and co-authors.: Description and Evaluation of the Characteristic of the NCAR High-Resolution Land Data Assimilation. *J. Appl. Meteorol. Clim.*, **46**, 694-713, https://doi.org/10.1175/JAM2463.1, 2007.

Cook, B. I., Bonan, G. B., and Levis, S.: Soil Moisture Feedbacks to Precipitation in Southern Africa. *J. Climate*, **19**, 4198-4206, 2006.

Cosgrove, B. A., and co-authors.: Land surface model spin-up behavior in the North American Land Data Assimilation System (NLDAS). *J. Geophys. Res.*, **108**(D22), doi:10.1029/2002JD003316, 2002.

Crosman, E. T., and Horel, J. D.: Sea and Lake Breezes: A Review of Numerical Studies. *Boundary-Layer Meteorol.*, **137**, 1-29, doi:10.1007/s10546-010-9517-9, 2010.

Dee, D. P., and co-authors.: The ERA-Interim reanalysis: configuration and performance of the data assimilation system. *Q. J. Roy. Meteorol. Soc.*, **137**, 553-597, doi:10.1002/qj.828, 2011.

Diallo, I., Giorgi, F., and Stordal, F.: Influence of Lake Malawi on regional climate from a double-nested regional climate model experiment. *Clim. Dyn*., **50**, 3397-3411, doi:10.1007/s00382-017-3811-x, 2018.

Diro, G. T., Raischer, S. A., Giorgi, F., and Tompkins, A. M.: Sensitivity to seasonal climate and diurnal precipitation over Central America to land and sea surface schemes in RegCM4. *Climate. Res*., **52,** 31-48, doi:10.3354/cr01049, 2012.

Estoque, M. A.: The sea breeze as a function of the prevailing synoptic situation. *J. Atmos. Sci*., **19**, 244-250, 1962.

Gleixner, S., Keenlyside, N. S., Demissie, T. D., Counillon, F., Wang, Y. and Viste, E.: Seasonal predictability of Kiremt rainfall in coupled general circulation models. *Environ. Res. Lett*., **12**, 114016, 2017.

Hong, S. Y., and Lim, J. O. J.: The WRF single-moment 6-Class microphysics scheme (WSM6). *J. Kor. Meteorol. Soc*., **42**, 129-151, 2006.

Hong, S. Y., and Dudhia, Y.: A new vertical diffusion package with an explicit treatment of entrainment processes. *Mon. Wea. Rev*., **134**, 2318-2341, 2006.

Huffman, G. J., Bolvin, D. T., Nelkin, E. J., Wolff, D. B., Adler, R. F., Gu, G., Hong, Y., Bowman, K. P., and Stocker, E. F.: The TRMM multisatellite precipitation analysis (TMPA): Quasi-global, multiyear, combined-sensor precipitation estimates at fine scales. *J. Hydrometeor*., **8**(1), 38-55, 2007.

Janjíc, Z.: The Step-Mountain Eta Coordinate Model: Further development of the convection, viscous sublayer, and turbulence closure scheme. *Mon. Wea. Rev*., **122**, 927-945, 1994.

Joseph, B., Bhatt, B. C., Koh, T.-Y., and Chen, S.: Sea breeze simulation over Malay Peninsula over an intermonsoon period. *J. Geophys. Res*., **113**, p.D20122, doi:10.1029/2008JD010319, 2008.

Jury, M. R.: Summer climate of Madagascar and monsoon pulsing of uts vortex. *Meteorol. Atmos. Phys.*, **128**, 117-129, doi:10.1007/s00703-015-0401-5, 2016.

Kain, J. S.: The Kain-Fritsch convective parameterization: an update. J. *Appl. Meteor.*, **43**, 170-181, 2004.

Kebede, S., Travia, Y., Alemayechu, T., and Marc, V.: Water balance of Lake Tana and its sensitivity to fluctuations in rainfall, Blue Nile basin, Ethiopia. *J. Hydrol.*, **316**, 233-247, 2006.

Keen, C. S., and Lyons, W. A.: Lake/Land Breeze Circulations on the Western Shore of Lake Michigan. *J. Appl. Meteorol.*, **17**, 1843-1855, 1978.

Kikuchi, K., and Wang, B.: Diurnal Precipitation Regimes in the Global Tropics. *J. Climate*, **21**, 2680-2696, 2008.

Kitoh, A., and Arakawa, O.: Reduction in tropical rainfall diurnal variation by global warming simulated by a 20-km mesh climate model. *Geophys. Res. Lett.*, **32**, L187709, doi:10,1029/2005GL023350, 2005.

Koseki, S., Koh, T.-Y., and Teo, C.-K.: Effects of the cold tongue in the South China Sea on the monsoon, diurnal cycle, and rainfall in the Maritime Continent. *Quart. J. Roy. Meteorol. Soc.*, **139**, 1566-1582, doi:10.1002/qj2025, 2013.

Koseki, S., and Bhatt, B. C.: Unique relationship between tropical rainfall and SST to the north of the Mozambique Channel in boreal winter. *Int. J. Climatology*, **38** (S1), e378-e387, doi:10.1002/joc5378, 2018.

Koseki, S., Pohl, B., Bhatt, B. C., Keenlyside, N., and Nkwinkwa Njouodo, A. S.: Insights into the summer diurnal cycle over eastern South Africa. *Mon. Wea. Rev.*, doi:10.1175/MWR-018-184-1, 2018.

Kruit, R. J. W., Holtslag, A. A. M., and Tijim, A. B. C.: Scaling of the sea-breeze strength with observations in the Netherlands. *Boundary-Layer Meteorol.*, **112**, 369-380, 2004.

Kumambala, P. G., and Ervine, A.: Water Balance Model for Lake Malawi and its Sensitivity to Climate Change. *The Open Hydrology Journal*, **4**, 152-162, 2010.

Lauwaet, D., van Lipzig, N. P. M., Van Weverberg, K., De Ridder, K., and Goyens, C.: The precipitation response to the desciccation of Lake Chad. *Quart. J. Roy. Meteorol. Soc.*, **138**, 707-719, 2012

Mak, M. K., and Walsh, J. E.: On the relative intensities of sea and land breezes. *J. Atmos. Sci.*, **33**, 242-251, 1976.

Mlawer, E., Taubman, S., Brown, P., Iacono, M., and Clough, S.: Radiative transfer for inhomogeneous atmosphere: RRTM, a validated correlated-k model for the long-wave. *J. Geophys. Res.*, **102**, 16663-16682, 1997.

Mooney, P. A., Mulligan, F. J., and Broderick, C.: Diurnal cycle of precipitation over the British Isles in a 0.44° WRF multiphysics regional climate ensemble over the period 1990-1995. *Clim. Dyn.*, **47**(9), 3281-3300, doi:10.1007/s00382-016-3026-6, 2016.

Mooney, P. A., Broderick, C., Bruyere, C. L., Mulligan, F. J., and Prein, A. F.: Clustering of Observed Diurnal Cycle of Precipitation over the United States for Evaluation of a WRF Multiphysics Regional Climate Ensemble. *J. Climate*, **30** (22), doi:10.1175/JCLI-D-16-0851.1, 2017.

Neuland, H.: Abnormal high water levels of Lake Malawi?- An attempt to assess the future behaviour of the lake water levels. *Geo J.*, **9**, 323-334, 1984.

Nikulin and co-authors.: Precipitation Climatology in an Ensemble of

CORDEX-Africa Regional Climate Simulations. *J. Climate*, **25**, 6057-6078, 2012.

Notaro, M., Holman, K., Zarrin, A., Fluck, E., Vavrus, S., and Bennington, V.: Infleuence of the Laurentian Great Lakes on Regional Climate. *J. Climate*, **26**, 789-804, 2013.

Pielke, R. A.: Influence of the spatial distribution of vegetation and soils on the prediction of cumulus convective rainfall. *Rev. Geophys*., **39**, 151-177, doi:https//doi.org/10.1029/1999RG000072, 2001.

Pitman, A. J., Avila, F. B., Abramowitz, G., Wang, Y. P., Phipps, S. J., and de Noblet-Ducoudré, N.: Importance of background climate in determing impacts of land-cover change on regional climate. *Nature Climate Change*, **1**, 472-475, doi:10.1038/NCLIMATE1294, 2011.

Pohl, B., Rouault, M. and Roy, S. S.: Simulation of the annual and diurnal cycles of rainfall over South Africa by a regional climate model. *Clim. Dyn*., **43**, 2207-2226, doi:10.1007/s00382-013-2046-8, 2014.

Reynolds, R. W., Smith, T. M., Liu, C., Chelton, D. B., Casey, K. S., and Schlax, M. G.: Daily high-resolution-blended analyses for sea surface temperature. *J. Climate*, **20**, 5437-5496, doi:10.1175/2007JCL1824, 2007.

Semazzi, F. H. M., and Song, Y.: A GCM study of climate change induced by deforestration in Africa. *Climate Research*, **17**, 169-182, 2001.

Schäfer, M. P., Ottfried, D., and Bniface, M.: Streamflow and lake water level changes and their attributed causes in Eastern and Southern Africa: state of the art review. *Int. J. Water Resour. D*., **6**, 853-880, doi:10.1080/07900627.2015.1091289, 2015.

Segele, Z. T., Lamb, P. J., and Leslie, L. M.: Large-scale atmospheric circulation and global sea surface temperature associations with Horn of Africa June-September rainfall. *Int. J. Climatology*, **29**(8), 1075-1100, 2009a.

Skamarock, W. C., Klemp, J. B., Dudhia, J., Gill, D. O., Barker, D. M., Duda, M., Huang, X. Y., Wang, W., and Powers, J. G.: A description of the advanced research WRF version 3. *NCAR technical note*, NCAR/TN/u201345?STR, 123pp, 2008.

Skofronick-Jackson, G., and co-authors.: The Global Precipitation Measurement (GPM) Mission for Science and Society. *Bull. Amer. Meteoro. Soc.*, 1679-1696, doi:10.1175/BAMS-D-15-00306.1, 2017.

Sousounis, P. J., and Mann, G. E.: Lake-Aggregate Mesoscale Disturbances. PartV: Impacts on Lake-Effect Precipitation. *Mon. Wea. Rev.*, **128**, 728-745, 2000.

Steyn, D. G.: Scaling the vertical structure of sea breezes revisited. *Boundary-Layer Meteorol.*, **107**, 177-188, 2003.

Stivari, S. M. S., de Oliveira, A. P., Karam, H. A., and Suares, J.: Patterns of Local Circulation in the Itaipu Lake Area: Numerical Simulations of Lake Breeze. *J. Appl. Meteorol.*, **42**, 37-50, doi:10.1175/1520-0450(2003)<0037:POLCIT>2.0.CO;2, 2003.

Sugimoto, S., and Takahashi, H. G.: Seasonal Differences in Precipitation Sensitivity to Soil Moisture in Bangladesh and Surround Regions. *J. Climate*, **30**, 921-938, doi:10.1175/JCLI-D-15-0800.1, 2017.

Teo, C.-K., Koh, T.-Y., Lo, J. C. F., and Bhatt, B. C.: Principal component analysis of observed and modeled diurnal rainfall in the Maritime Continent. *J. Climate*, **24**, 4662-4675, 2011.

Thiery, W., Davin, E. L., Seneviratne, S. I., Bedka, K., Lhermitte, S., and van Lipzig, N. P. M.: Hazardous thunderstorm intensification over Lake Victoria. *Nat.*

Communication, **7**, 12786.

Tyson, D. P.: Nocturnal local winds in a Drakensberg Valley. *South African Geographical Journal*, **50**, 15-32, 1968a.

Tyson, D. P.: A Note on the Nomenclature of the Topographically-induced Local Winds of Natal. *South African Geographical Journal*, **50**, 33-34, 1968b.

Viste, E., and Sorteberg, A.: The effect of moisture transport variability on Ethiopian summer precipitation. *Int. J. Climatology*, **33**, 3106-2123, doi:10.1002/joc.3566, 2013.

Walker, J., and Rowntree, P. R.: The effect of soil moisture on circulation and rainfall in a tropical model. *Quart. J. Roy. Meteorol. Soc.*, **103**, 29-46, 1977.

Wely, O. L. F., Ribbink, A. J. and Tweddle, D.: Lake Malawi: fishes, fisheries, biodiversity, health and habitat. *Aquat. Ecosyst. Health Manag.*, **13**:3, 241-254, doi:10.1080/14634988.2010.504695, 2010.

Xu, L., Liu, H., Du, Q., and Wang, L.: Evaluation of the WRF-lake model over a highland freshwater lake in southwest China. *J. Geophys. Res. Atmos.*, **121**, 13,989-14,005, doi:10.1002/2016JD025396, 2016.

Yang, G., and Slingo, J.: The diurnal cycle in the tropics. *Mon. Wea. Rev.*, **129**, 784-801, doi:10.1175/1520-0493(2001)129<0784:TDCITT>2.0CO;2, 2001.

Figures

(a)

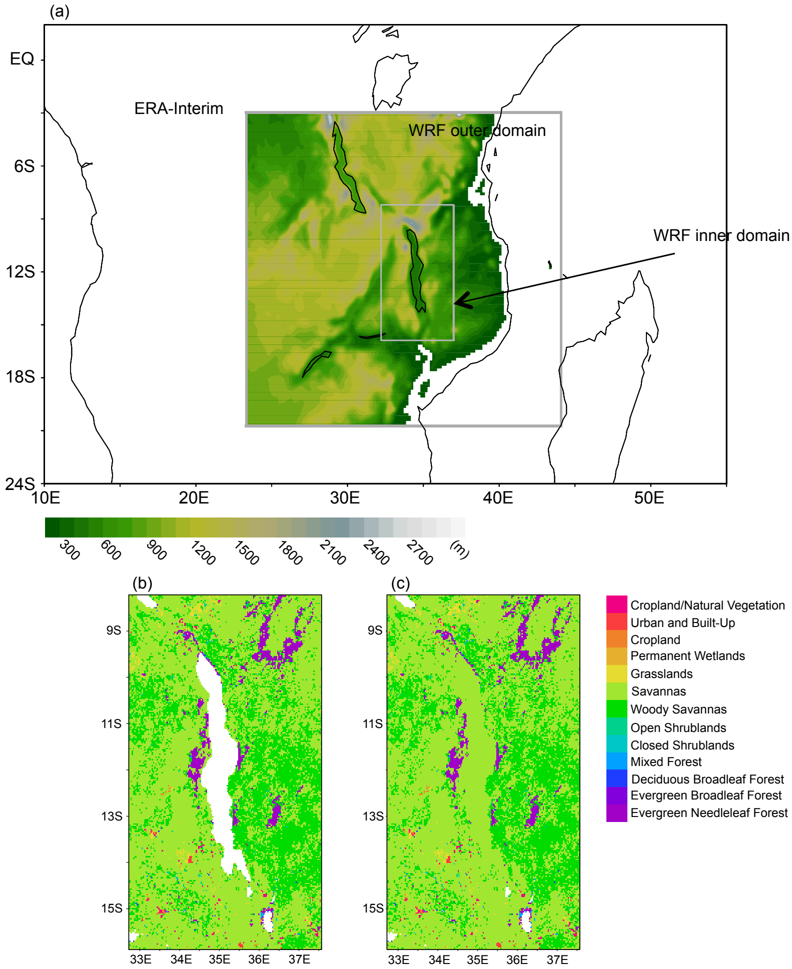

Figure 1.
(a) Domains for WRF simulations with terrain height obtained from GTOPO30. (b) and (c) landuse index of the boundary condition for the inner domain of WRF-CTL and WRF-NOLM, respectively

816

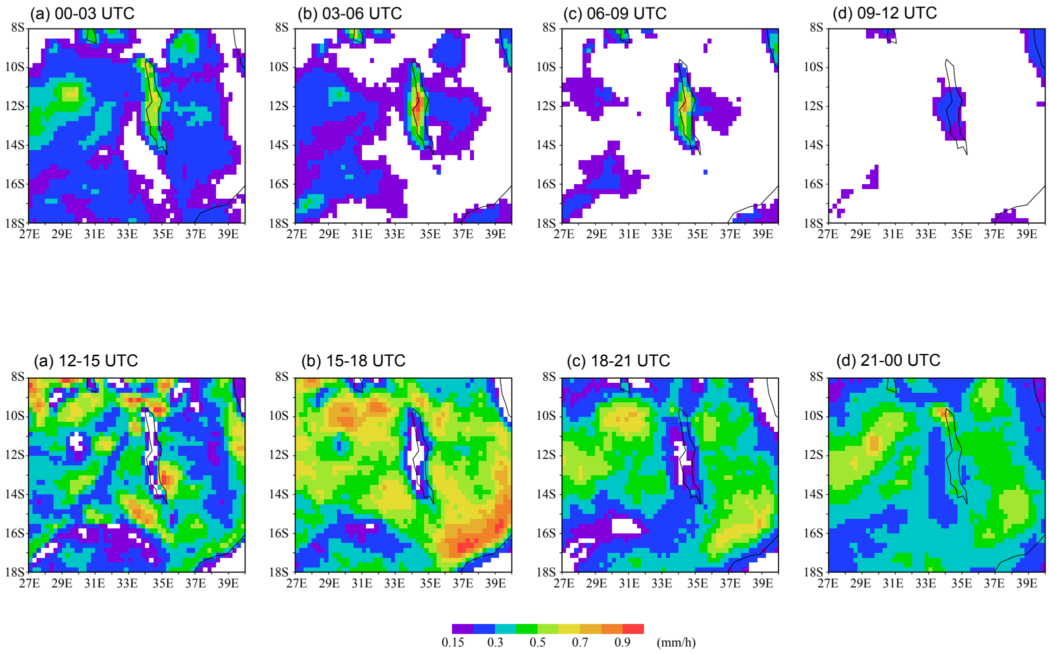

Figure 2.
Climatological 3-hourly precipitation of TRMM-3B42 in NDJFM (1998-2012). The white color is precipitation less than 0.15mm/h.

817

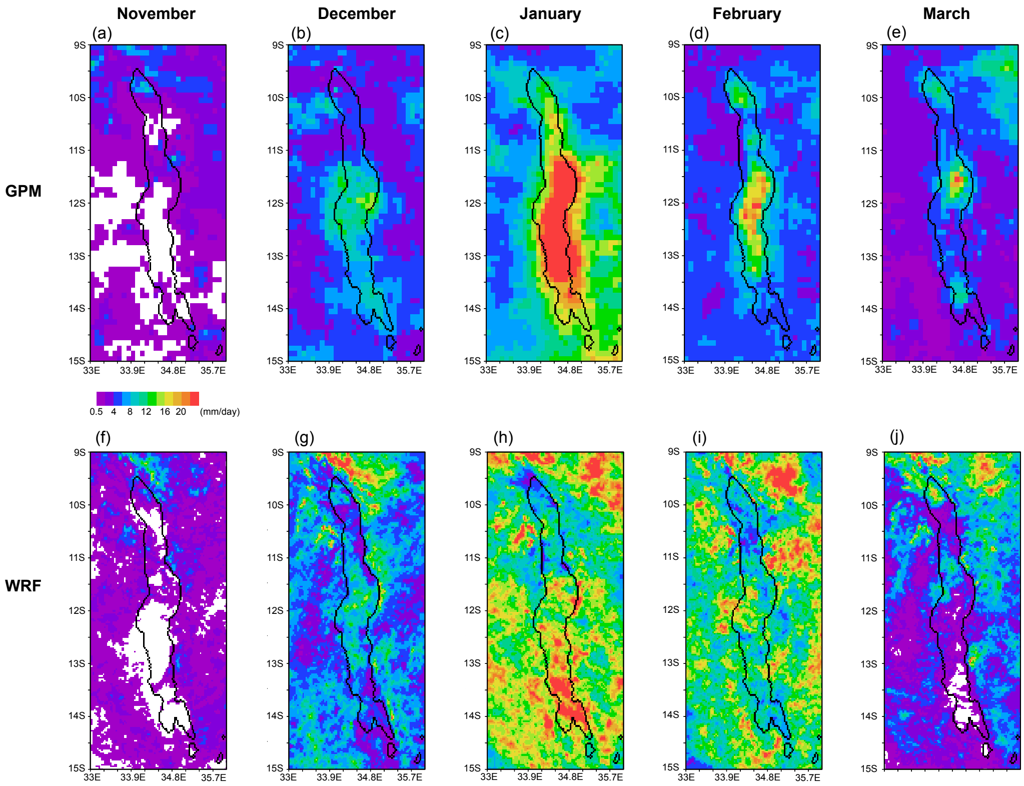

Figure 3.
Monthly-mean precipitation of (top) GPM and (bottom) WRF-CTL from November to March in 2014/15. The white color is precipitation less than 0.5 mm/day.

818

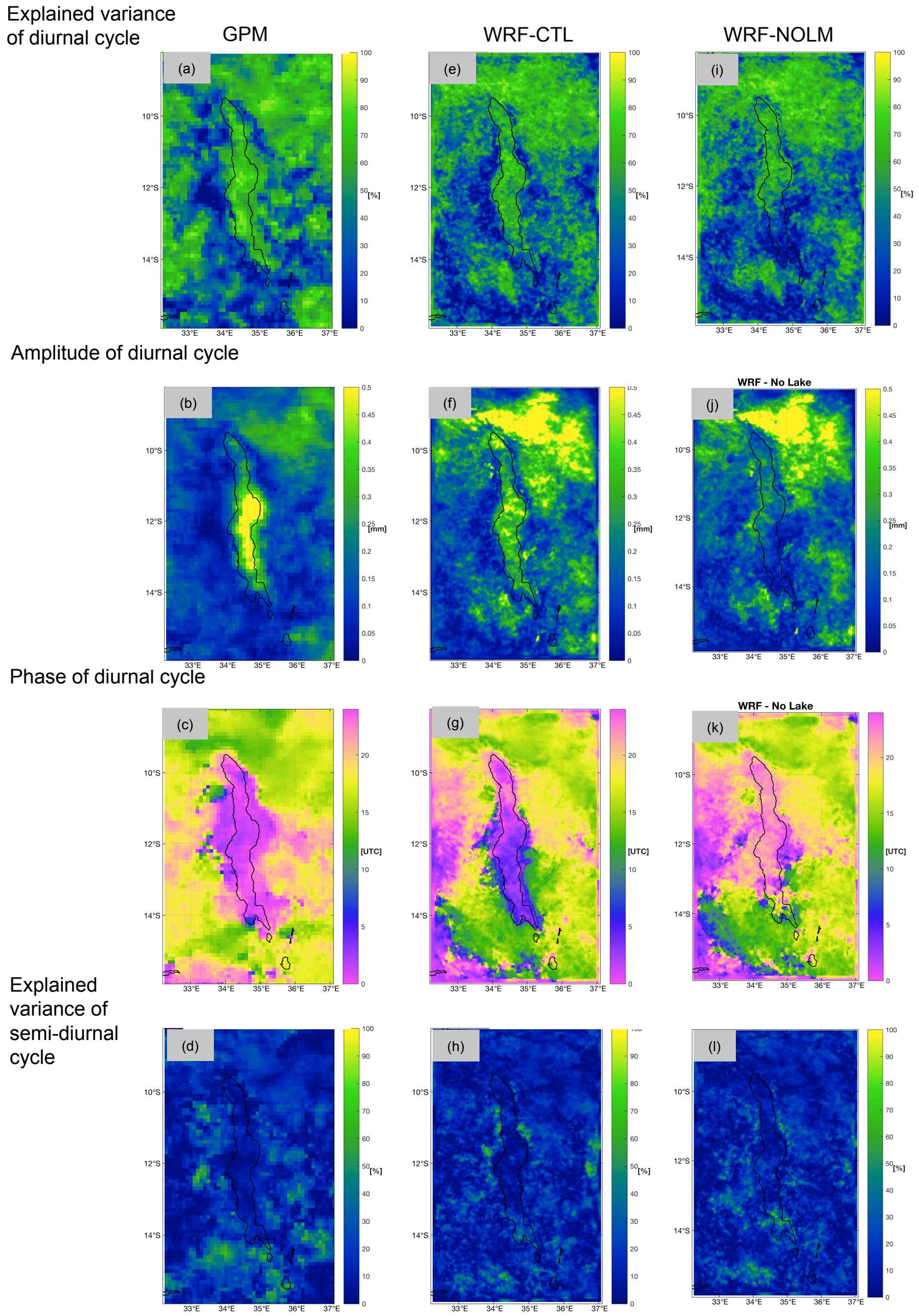

Figure 4.
Characteristics of daily-scale temporal variation in precipitation estimated by harmonic analysis for (1st row) explained variance of diurnal cycle, (2nd row) amplitude of diurnal cycle, (3rd row) phase of diurnal cycle, and (4th row) explained variance of semi-diurnal cycle for (left) GPM, (middle) WRF-CTL, and (right) WRF-NOLM, respectively.

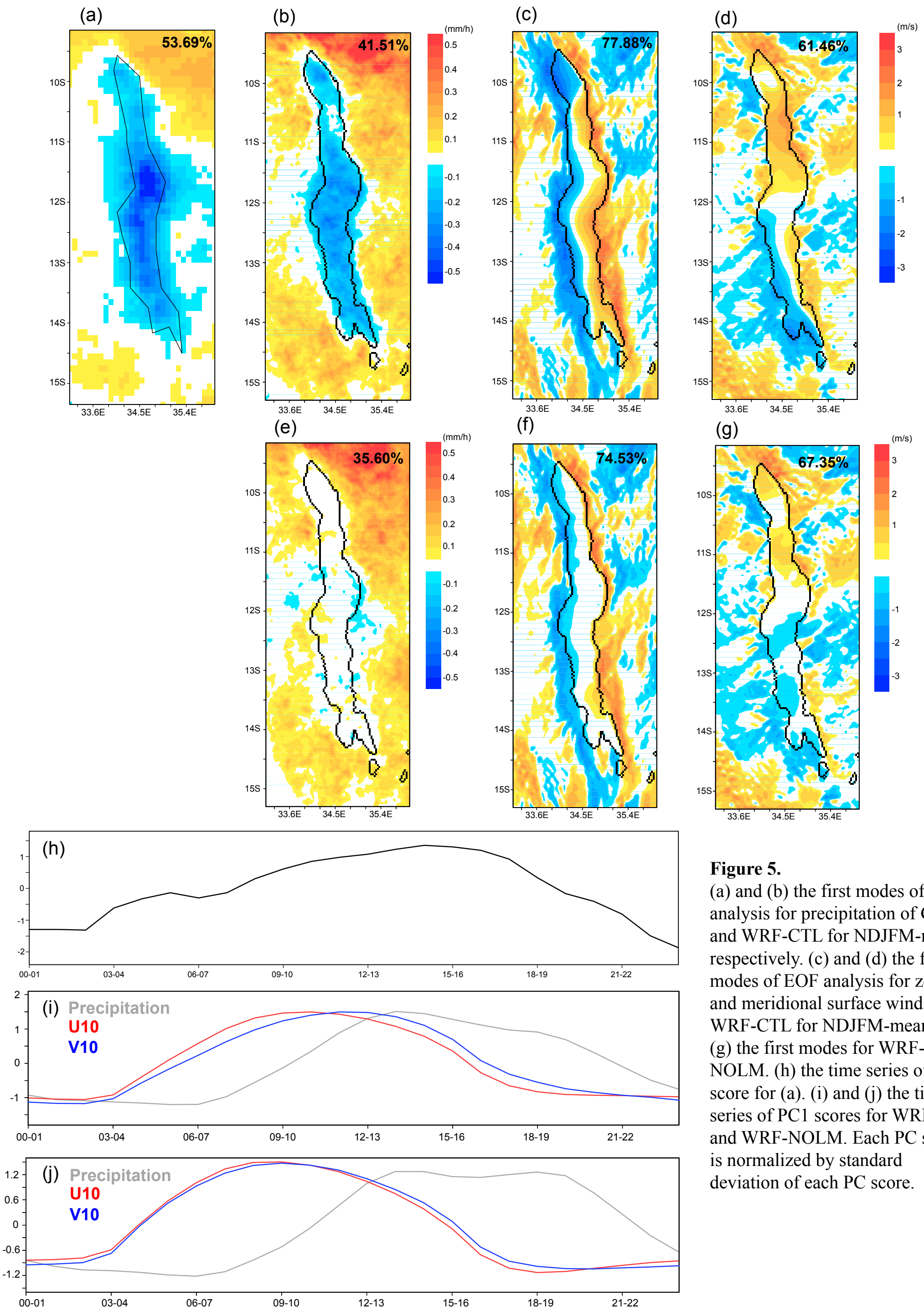

Figure 5.
(a) and (b) the first modes of EOF analysis for precipitation of GPM and WRF-CTL for NDJFM-mean, respectively. (c) and (d) the first modes of EOF analysis for zonal and meridional surface winds of WRF-CTL for NDJFM-mean. (e)-(g) the first modes for WRF-NOLM. (h) the time series of PC1 score for (a). (i) and (j) the times series of PC1 scores for WRF-CTL and WRF-NOLM. Each PC score is normalized by standard deviation of each PC score.

825

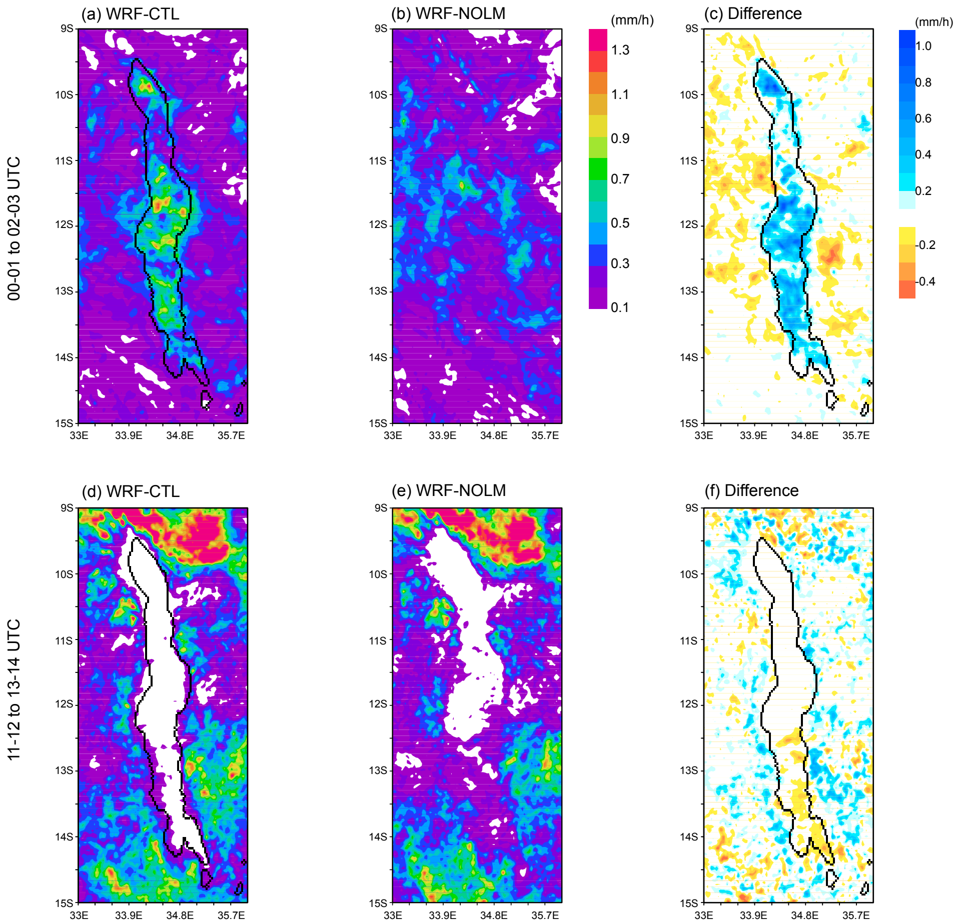

Figure 6.
Nighttime mean of precipitation of WRF-CTL and WRF-NOLM in (a) and (b), respectively and its difference (WRF-CTL minus WRF-NOLM) in (c). (d)-(f) same as (a)-(c), but for daytime mean.

826

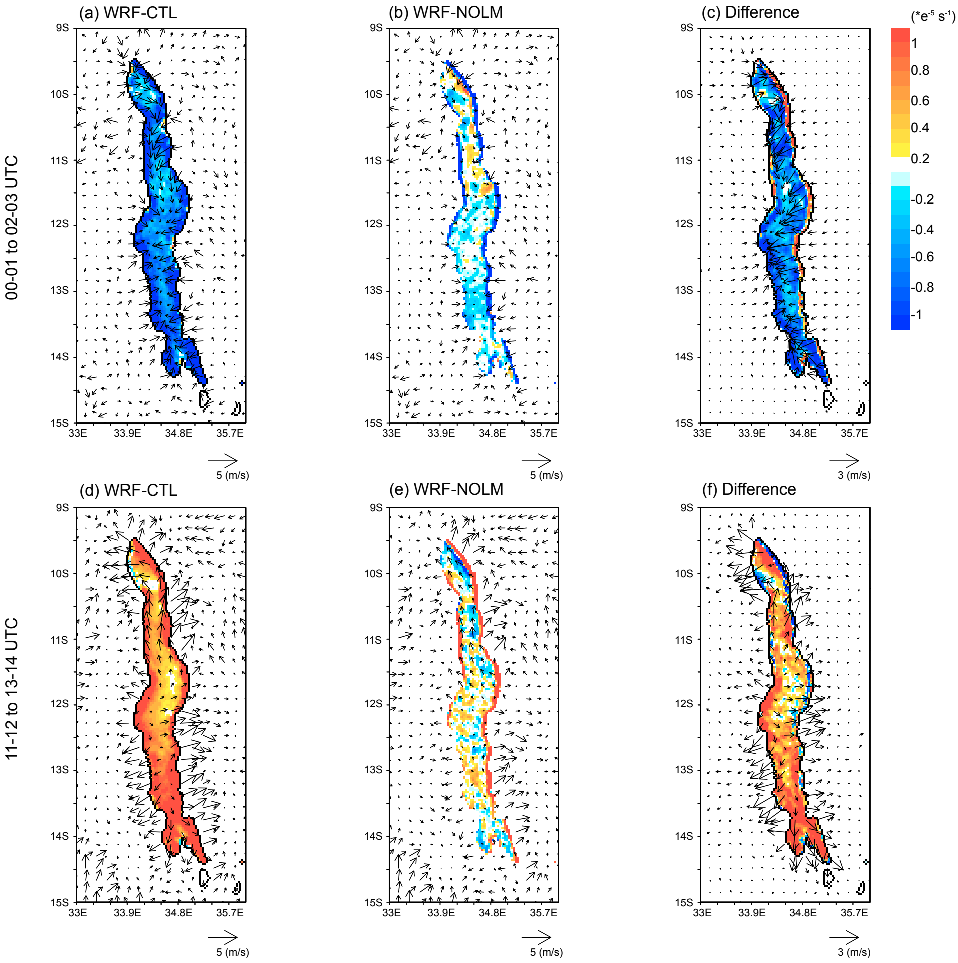

Figure 7.
Same as Fig.6, but for surface horizontal winds (arrows) and its divergence (color). Note that the surface winds and its divergence are anomalies from daily-mean values.

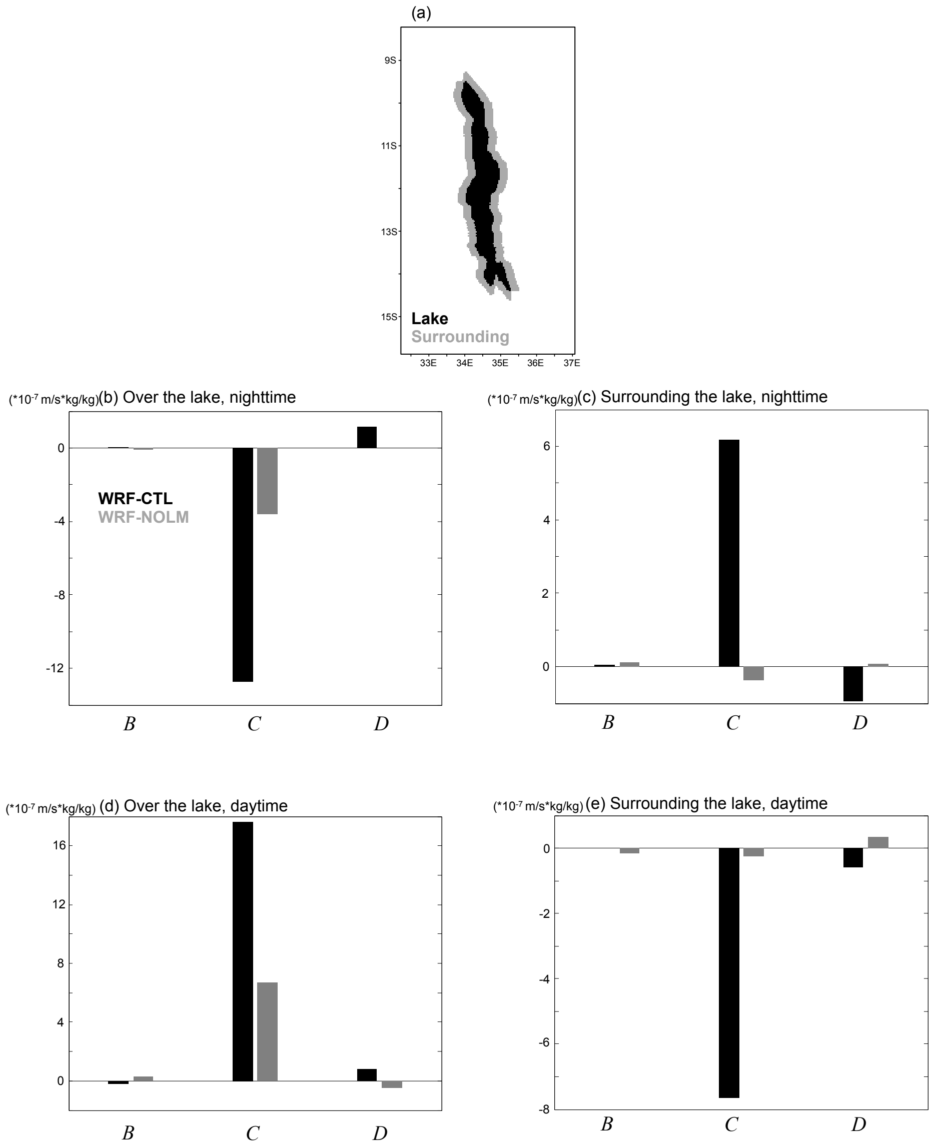

Figure 8.
(a) Grids of the lake (black) and surrounding area (gray) for area-averaging. The area-averaged three components of moisture flux divergence in the equation 3 for (b) over the lake, nighttime (00-01 to 02-03 UTC), (c) surrounding the lake, nighttime, (d) over the lake, daytime (11-12 to 13-14 UTC), and (e) surrounding the lake, daytime for WRF-CTL (black) and WRF-NOLM (gray), respectively.

831

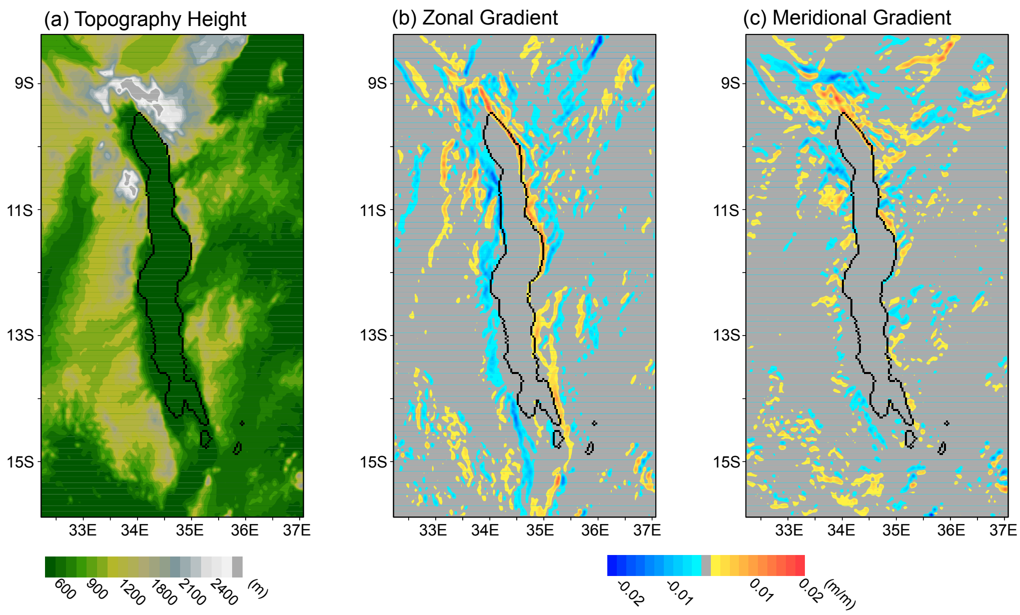

Figure 9.
The distribution of topography around Lake Malawi. (a) Topographic altitude in WRF inner domain and its zonal and meridional gradients in (b) and (c).

832